LOWER LEG INJURIES CAUSED BY DYNAMIC AXIAL LOADING AND MUSCLE TESTING

Yuichi Kitagawa
Hideaki Ichikawa
Chinmoy Pal
Nissan Motor Co., Ltd.
JAPAN
Albert I. King
Robert S. Levine
Wayne State University
USA
Paper Number 98-S7-O-09

ABSTRACT

The effect of muscular tension on lower leg injuries was investigated in this study. Rigid body simulation was used to examine the kinematics of an occupant making a braking during a frontal crash. Muscular tension was reproduced by constant spring elements defined in the lower leg. Simulation results showed that tibial axial load was increased by the muscular tension. A series of cadaver tests was conducted to study the effect of muscular tension in detail. Dynamic axial loading was applied to human specimens with a pendulum hitting at approximately 3 m/s. The test condition represented loading to a driver's right foot stepping on a brake pedal and struck by a toe board. The metatarsal heads were placed on the brake pedal and an initial tensile force was applied on the Achilles tendon. Sixteen tests were performed on eight pairs of cadeveric lower legs. There was a significant increase in the tibial axial load in comparison with the impact load because of preloading by muscular tension. Tibial pylon fracture, which is one of the severest forms of injury of the lower leg, was frequently observed in these tests. Although the fracture load level in the tibia was almost the same as that reported in previous studies, this study shows that less external force is required to cause tibial pylon fractures with muscular tension.

INTRODUCTION

The proper use of restraint systems such as seat belts and airbags can reduce the risk of upper body injuries in frontal crashes. Although misuse of restraint system is still observed in the field and airbag aggressiveness is a problem, the consequences must be recognized and improvements need to made. As for lower leg injuries, there is no effective countermeasure which has been proven to reduce injury risk. This is due to a lack of information on the injury mechanism. What happens exactly to the lower legs during a crash and the relationship between loading condition and injury mode are not well understood.

The first approach was to review statistical data for lower leg injuries. In an analysis of NASS data from 1979-1986, Morgan (1991) reported that lower leg injury amounted to 25% of all body regions for non-belted occupants and almost the same percentage for belted occupants. The analysis also showed that ankle and foot injuries accounted for a large proportion of lower leg AIS2+ injuries. Crandall (1994) examined 1990-1992 NASS files and reported that upper and lower extrimity injuries are still frequently seen in drivers protected by airbags while head and neck injuries decreases in comparison with cases without the airbag. Otte (1992) studied the types of ankle and foot injuries based on data from 140 belted drivers between 1985-1990. The research was carried out by the traffic accident research unit of Hannover. The ankle joint was the most commonly injured area with a rate of 37.1% followed by the metatarsal bone with a rate of 36.1%. As far as brake pedals are concerned, Morgan (1991) also reported that 57% of drivers' ankles were injured while the foot was on the pedal based on his analysis of NASS data from 1979-1986. Thomas (1995) examined the CCIS database and noted that injury to the driver's right leg is increased by a brake pedal when there is 200 mm of footwell intrusion. Increased injury risk due to pedal interaction with the leg was pointed out in those studies. The brake pedal is, however, not the only cause of lower leg injury of course. External forces on the foot can be caused not only by pedal interaction but also by inertia or intrusion.

Another approach is to determine threshold of each injury by means of impact biomechanics. Currently, external forces due to inertia or intrusion are considered to be the major cause of ankle and foot injuries. Begeman investigated the impact response of human ankle in dorsiflexion and found 45 deg. to be the injury threshold (1990). He also reported that the threshold of inversion and eversion was 60 deg. (1993). As for tibial injury involving the ankle joint, a number of axial loading tests has been done. Yoganandan (1996) summarized tibial axial loading tests done at Wayne State University, CALSPAN and the Medical College of Wisconsin. He reported that the load

for a 50% probability of fracture in the lower leg was estimated to be 6.8 kN. Klopp (1997) loaded fifty lower legs including the midshaft of femur. A linear logistic model revealed that 9.3 kN of contact force to the foot gave a 50% probability of injury. In terms of fracture mode, however, it has not been determined yet what loading condition is likely to cause each fracture mode. A common finding in previous studies was that calcaneal fracture was most likely to occur when the foot was impacted by a pendulum.

From the medical point of view, ankle injury is a most important subject because it is the weakest area in the lower leg and it sometimes results in long-term disability or impairment. Levine (1986) noted that tibial pylon fractures, which involve the ankle joint, require several months of medical treatment and the result tends to be poor. It is rated as one of the severest forms of lower leg injury. Pylon fractures can occur when the distal tibia is pushed very hard and upward by the talus but it has been difficult to reproduce in laboratory tests because calcaneal fracture is more likely to occur under a direct impact. Begeman (1997) conducted a series of dynamic loading tests on lower legs and found pylon fractures were generated at loads between 6 and 9 kN. He saw some pylon fractures when he removed the foot before applying the load and only one pylon fracture was observed with the foot in place. Likewise just one leg sustained a pylon fracture out of fifty specimens studied by Klopp (1977). Thus the injury mechanism causing tibial pylon fractures is not well understood.

In this study, it is hypothesized that muscular force generated in braking can increase the risk of tibial pylon fracture. When a driver's right foot is stepping on the brake pedal, the Achilles tendon pulls on the calcaneus due to muscular contraction of the calf muscles, generating preloading to the tibia. External forces could be applied to the forefoot by the pedal or the toe board coming backward after a frontal crash occurs. As mentioned in the review of analyses of accident data, there is evidence that the driver's right leg is at more risk than the left, due in part to muscular tension, intrusion and pedal interaction. A rigid body simulation using MADYMO was used to determine the kinematics of a driver's legs with muscular tension during a frontal crash. Constant spring elements were used to simulate muscular activity in the right leg. The effect of muscular tension can be examined by comparing the tibal axial load with another model without muscular tension. The simulation results could possibly reveal a mechanism for tibial pylon fracture. Then a series of cadaver tests using human specimens was conducted to confirm the hypothesis and determine the effect of muscular force combined with an external force. Because entrapment of the knee by the lower dashboard can be another factor to increase the compressive force to the tibia, this study is limited to a simple pendulum impact to a tibial/foot specimen fixed to a wall.

RIGID BODY SIMULATION

Simulation Model

Numerical simulations were performed using MADYMO Ver. 5.2. A Hybrid III Dummy Model develped by TNO was used because no humanly model was available and the dummy model would be adequate for an examination of the basic kinematics of a driver with muscular tension. The model is shown in Figure 1. Typical dimensions of a passenger car were used to the vehicular interior, such as a seat, a steering wheel and an instrumental panel. The driver's seat was equipped with a 3-point belt and an air bag system. A brake pedal was placed above the toe board. Friction factors were assigned to the toe board, floor, pedal and seat pan. Three Kelvin elements were introduced to represent the muscle forces in the calf, femur and hip. Braking was simulated by an initial contraction of these Kelvin elements. A force balance between these spring elements and the occupant was maintained to simulate this bracing motion.
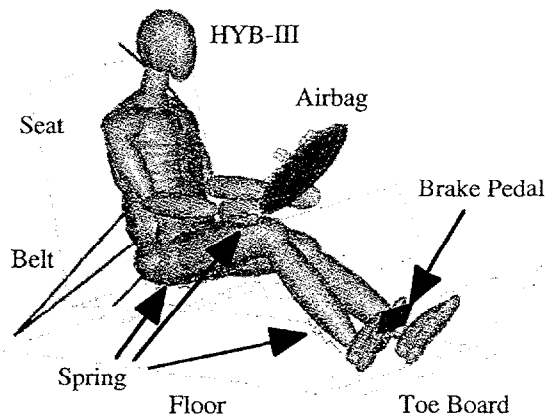
Figure 1. Rigid Body Simulation Model.

A stability analysis was conducted to obtain a quasi-static balance of the muscle forces. In the stability analysis, a linear and very stiff force-displacement curve was defined for each spring element. Then the brake pedal was moved rearwards so that it pushed against the forefoot. The contact force between the pedal and the forefoot constituted the pedal force while the tensile forces in the spring elements were the muscle forces that reacted against the applied pedal force. Figure 2 shows the relationship between the pedal force and the muscle forces from this stability analysis. For a given pedal force in this plot, the necessary force levels can be determined for each of the three muscle springs. An interesting result in this stability analysis was that both the muscle force and the joint moment were the largest at the ankle. It means that the response of the calf muscles is the most important under a set of given conditions. In this simulation, a pedal force of 1.0 kN was assumed. The corresponding forces in the calf, femur and
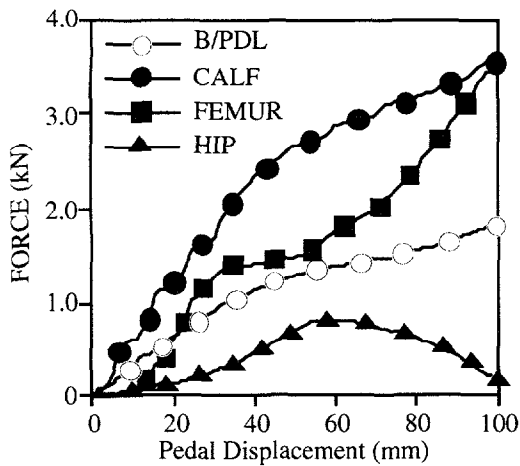
Figure 2. Force Balance of Muscle Springs.
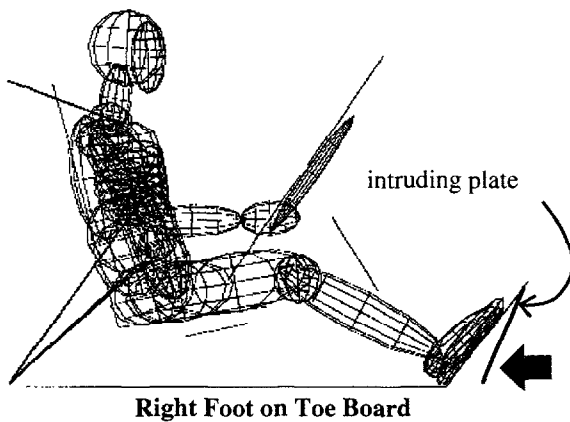
Right Foot on Toe Board
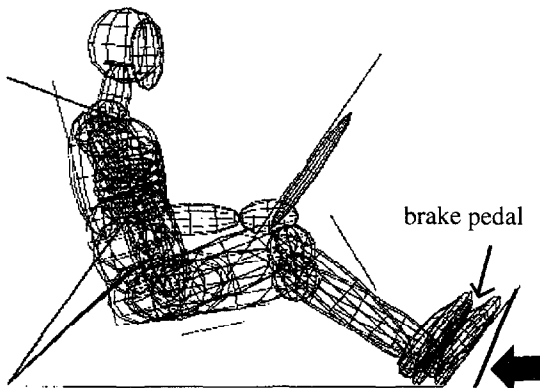
Right Foot on Brake Pedal

Figure 3. Models with Different Foot Position.

hip muscles were determined as 2.0 kN, 1.3 kN and 0.33 kN respectively, as shown in Figure 2. This condition only represents one possible case. Forces in a real situation can change depending on driving posture and the geometry of the vehicular interior. Thus, no attempt was made to validate this model.
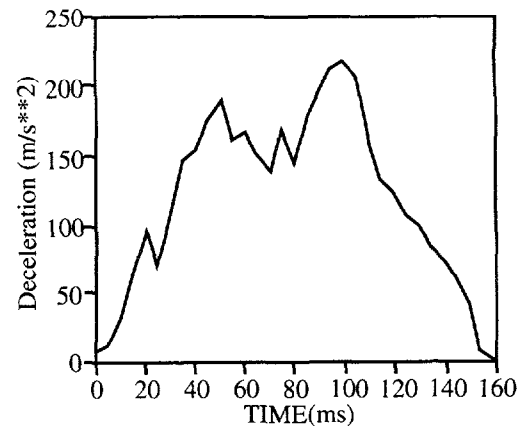
Figure 4. Vehicle Body Deceleration.
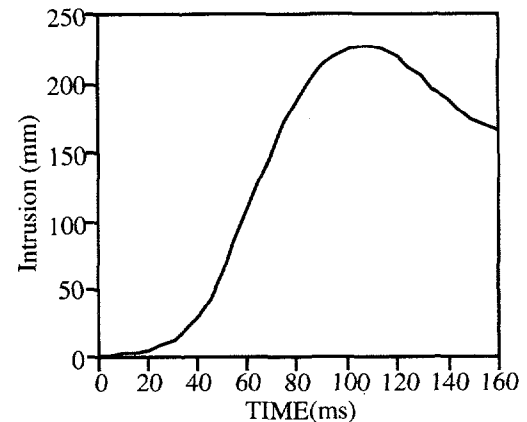
Figure 5. Intrusion of Toe Board.

Figure 3 shows two different models used in dynamic simulations. Both legs of the dummy were placed on the toe board in the first model whereas the right foot was on the brake pedal in the second model. Muscle force was not applied in the first model while the forces specified above were applied to the Kelvin elements in the second model. There is a toe board under the feet and another plate was defined to reproduce the intrusion. A steeper angle was used for this plate because the intrusion is generally larger in the upper area of the footwell. The deceleration due to a frontal crash was given to the dummy as a forward acceleration. Figure 4 shows a typical vehicular deceleration pulse for a car-to-car frontal offset crash test. The intrusion curve, as shown in Figure 5, was obtained from a numerical simulation of an offset deformable barrier crash and given to the movable toe board.The lateral component of deceleration and intrusion were neglected for simplicity. The following conditions were considered.

Case 1: No muscle force, Feet on the toe board.
Case 2: No muscle force, Right foot on the brake pedal.
    (same as Case 3 but no Kelvin elements)
Case 3: Muscle forces acting, Right foot on the brake pedal.

Simulation Result

Figure 6 shows dummy kinematics from 0 to 110 ms in Cases 1 and 3. Symmetric motion was observed in Case 1 because both dummy legs were placed on the toe board. With the right foot on the brake pedal in Case 3, larger dorsiflexion occurred in the right ankle as the pelvis moves forward due to inertia. Rotation of the right ankle was larger than those of the other leg joints. The contact between the dummy's right foot and the intruding toe board occurred at between 50 and 60 ms after the impact in Case 3. An external force should act on this foot after that time. Because the heel could slide forward on the floor in this simulation, the contact occurred at the heel. The timing of the contact was slightly different with and without muscles because of the difference in the rate of rotation of the right ankle. It could also change with the distance between the pedal and the toe board or with the speed of intrusion. The knees hit the bolster at around 70 ms and the maximum displacement of the pelvis was seen at about 110 ms.

Figure 7 shows the tibial axial force-time histories calculated for the right leg. The effect of braking can be seen by comparing these plots. Cases 2 and 3 have prominent peaks in the right tibial forces whereas there are only two mild peaks in Case 1. The first peak in Case 1 was probably due to the deceleration of the dummy and the second peak was due to both deceleration and the intrusion force. The maximum force occurred at 60 ms in Cases 2 and 3. This corresponds to the time of the contact between the foot and the toe board. Since the only difference between Cases 1 and 2 is the position of the right foot, that position is the major cause of the large force peak in Case 2. The effect of foot position can be also confirmed by comparing with the force curve for the left leg shown in Figure 8. Similar force curves were obtained for the left leg in all these cases. Going back to the forces on of the right leg, the maximum tibial axial force was about 2.0 kN in Case 1 at 85 ms after the impact whereas it reached 3.0 kN at about 60 ms in Case 2. The larger peak force in Case 3 indicates the effect of muscular tension on the tibial axial force. It is quite similar to that of Case 2 but the peak was increased by 1.5 kN to 4.5 kN at 60 ms. This is because of muscular tension due to braking. The additional tibial axial force increases the risk of tibial injury. However, 4.5 kN of tibial force is still smaller than the threshold values proposed in previous studies. A more severe impact may be needed to cause fracture and entrapping of the knee by the lower dashboard could be factors which can increase the tibial axial force. The plot in Figure 8 indicates that the intrusion is the dominant cause of the second force peak in the left leg. Figure 9 shows the contact force-time histories for the right foot due to the intruding toe board in Cases 2 and 3. The external force was produced by the heel contact as mentioned before. The force curves appear similar to those for the tibial axial force except
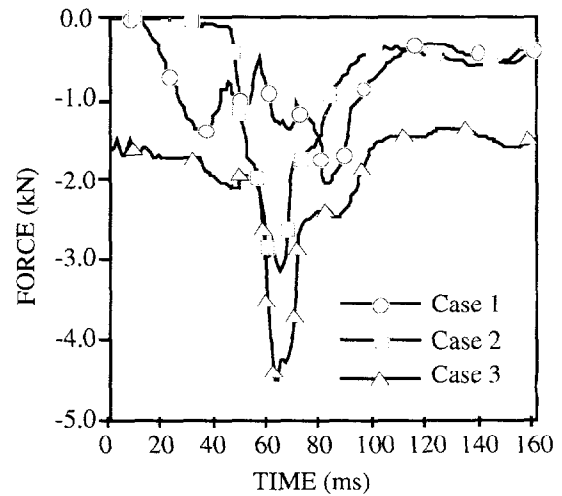
Figure 7. Axial Load on Right Tibia.
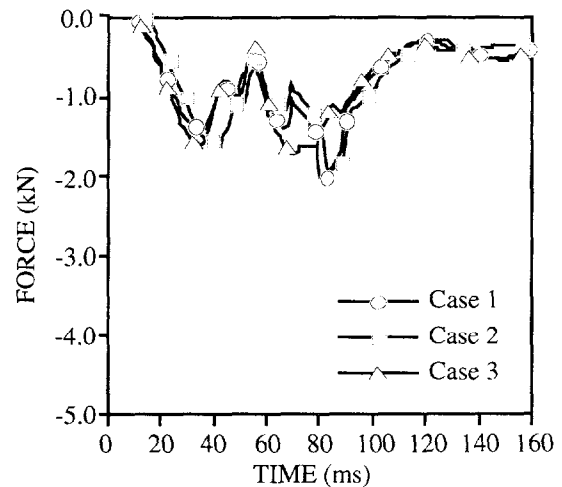
Figure 8. Axial Load on Left Tibia.
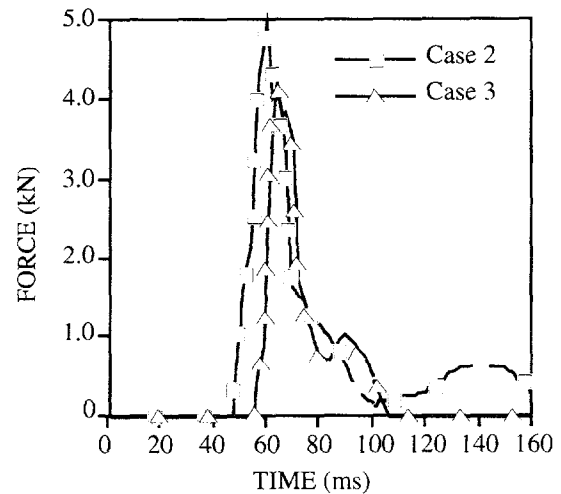
Figure 9. Contact Force on Right Foot.

1600
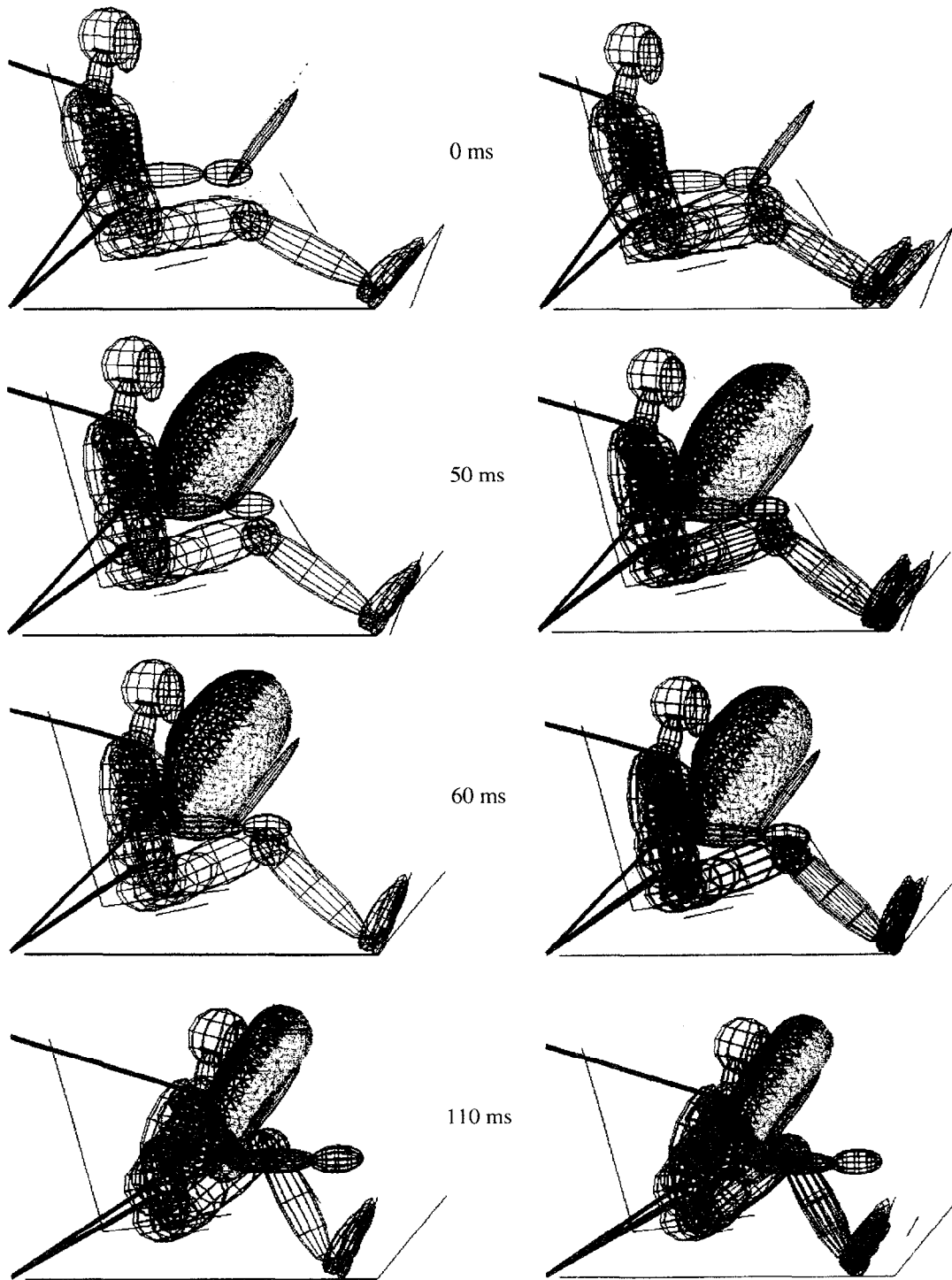
Case 1: No Muscle Force, Foot on Board   Case 3: With Muscle Force, Foot on Pedal

Figure 6. Dummy Motion in Time Frames: With and Without Muscle/Intrusion.

for preloading. The large force peak in Case 2 means that the external force due to intrusion was not influenced much by the muscular tension.

Simulation results suggest that both muscular tension and external force due to intrusion can increase the axial force in the right tibia whereas the external force also determines the impact severity to the foot. As the driver steps on the brake pedal stronger, the preloading to the tibia increases. If an additional external force works on the foot, the tibia may be compressed more. The intrusion means not only its deformation but also its velocity. Since the force peaks appear at around 60 ms, the final amount of intrusion does not seem to be a major factor causing lower leg injuries. Figure 10 shows the time histories of the pedal force, the contact force and the tibial axial force of the right leg. The compressive force through the tibia in negative direction was reversed to positive for comparison. It is obvious that the tibial axial force is the sum of the muscular tension force and the external force. Figure 11 shows the velocity change in the intruding plate and the right foot in Cases 1 and 3. A positive velocity means a forward movement relative to the vehicle. The velocity of the intruding toe board was measured at the same height as that of the heel. Intrusion started at 55 ms. When the foot was on the toe board in Case 1, the heel was pushed away as the toe board moved backwards, finally reaching the same velocity as the intruding plate. The velocity change was 4.76 m/s. In Case 3, the heel had 2.75 m/s of forward velocity at 55 ms because it was sliding on the floor. This resulted in a larger velocity change of 9.3 m/s, which was almost twice of that in Case 1. But it should be still even larger without the positive motion of the heel. Although the velocity curve for Case 2 is not shown in Figure 11, a similar curve is expected based on the similarity of the contact force curves.

Some interesting issues have been raised by the simulation study. The external force due to intrusion could be the major cause of injury. The severity of the external force is determined by the foot position and intrusion speed. The calcaneus was the first contact area in this simulation. A direct impact to the heel is likely to cause a calcaneus fracture. It could be the reason why calcaneal fractures are frequently seen in real crashes. However, care must be taken as to how the external force acts on the foot. The foot was treated as a rigid body in this simulation and the toe board was defined as a flat plate. Heel contact was the most likely to occur under this condition. A real human foot can deform when the pedal pushes the forefoot back and the toe board may not be flat after a collision. The brake pedal also moves backwards and pushes on the forefoot in some cases. The external force due to intrusion, therefore, can act anywhere on the foot. Another issue is that the muscular tension generates preloading of the tibia. If the external force acts on the foot in the presence of preloading, the tibia can be under more compression and can be fractured if the impact
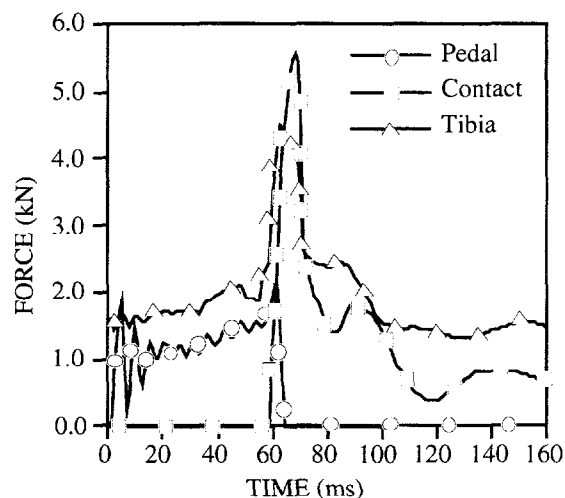
Figure 10. Force on Pedal/Heel/Tibia.
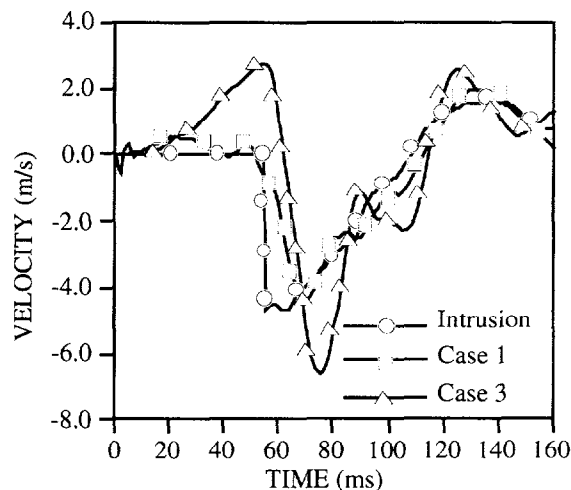
Figure 11. Velocity Change of Foot / Plate.

is severe enough. Furthermore, if the external force is applied to the forefoot, the tibia can be fractured without calcaneal fracture. This mechanism can explain why few pylon fractures are seen in laboratory tests despite the fact they are actually seen in real crashes. An in-depth analysis is necessary to understand the injury mechanism of the human foot and ankle complex under a combined loading by muscular tension and external force. Cadaver tests described below were conducted for this purpose.

CADAVER TESTS

Procedure

Eight pairs of human cadaveric lower legs were obtained for this study through the willed body programs of Wayne State University and the University of Michigan. Table 1 lists the cadavers used. Their age ranged from 59 to

1602

83 years with an average of 71. Six of the eight cadavers were female. A total of sixteen specimens was used in the tests. All specimens were examined radiographically and physically before testing to confirm that there were no anatomic and pathologic abnormalities. Each specimen was cut distal to the knee. The length of each specimen was 300 mm and about 100 mm of soft tissue was removed from the proximal tibia for potting. The Achilles tendon was dissected free and placed into a tendon catcher made of steel mesh (finger trap). The tendon catcher tightens around the tendon as it is pulled. The maximum force it can generate depends on how slippery the tendon is. Polyester suture, Ethibond B-499, was used to increase this force. The tendon was stitched by passing the suture through the mesh of the catcher as shown in Figure 12. The suture helped increased the tendon force up to several kilo Newtons. The proximal end of the tibia was potted in a fiber reinforced epoxy block. This condition represents the entrapment of the knee by the lower dashboard. Although the condition did not allow the relative motion between the tibia and fibula, it was accepted because generally the fibula does not contribute much to the strength of the lower leg.

Figure 13 is an schematic view of the entire test apparatus. The pot was attached rigidly to the fixture. The tibial axis was adjusted to lie along a horizontal line. A rigid pendulum weighting 18 kg was used to impact the bottom of the foot. The impactor was cylindrical with a diameter of 70 mm. The height of the centerline of the pendulum was 50 mm lower than the tibial axis. This impact provided the external force to the forefoot. Half an inch of ensolite padding was used on the impactor head to damp out high frequency vibrations. An aluminum plate was fixed to the sole of the foot to prevent direct contact of the foot by the impactor. Another aluminum plate was anchored to the test fixture to keep the foot plate from rotating. When the tendon force was applied, the forefoot was resisted by this plate.

A constant tendon force was maintained by the use of an energy absorber (EA) in the form of 2 aluminum plates, which tore at a constant load as shown in Figure 14. The Y-shaped plate yielded under a constant force when the both ends were pulled. When a couple of the aluminum plates were tested, the static tearing force was 1.4 to 1.6 kN. Due to strain rate dependency, the dynamic force was expected to be 10-20% higher but almost constant. An electrically

Table 1. Cadaver Properties

CAD#	AGE	SEX	Death Date	Cause of Death
271	68	F	1995/12/19	Hepatic Coma
242	69	F	1995/10/01	Acute Myocardial Infaction
715	59	M	1992/09/05	Massive Intracranial Bleeding
28483	75	F	1997/03/11	Respiratory Failure
28443	83	F	1997/03/02	Arteriosclerotic Caroiovascular Disease
28441	69	F	1997/03/04	Advanced Cervical Carcinoma
900	75	M	1993/08/15	Pneumonitis
480	70	F	1997/02/02	Cardiac Arrythmia

Figure 12. Tendon Catcher.
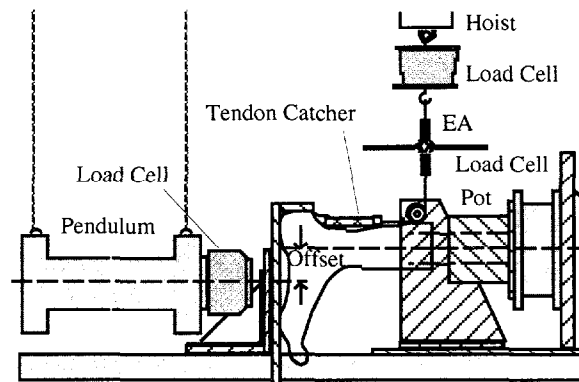
Figure 13. Dynamic Loading Apparatus.

powered hoist was used to apply a tensile force to the Achilles tendon through a cable. The tensile force, checked by a load cell placed between the EA and the hoist, was increased until the EA started tearing. The foot plate was kept perpendicular to the tibia during preloading. Then the pendulum was accelerated by a pneumatic cylinder and impacted the foot plate at approximately 3 m/s. A load cell and an accelerometer were mounted on the pendulum to provide a mass corrected impacting force. The tibial force and moment were measured by a 6-axis load cell behind the pot. The analog data were filtered and digitized at 10000 samples per second and were processed as channel class 1000 data. A 16 mm high-speed camera running at 500 fps was used to analyze the motion of foot to which photo targets had been applied. The time of impact was recorded by an electrical signal on the data acquisition system and by a synchronized flash for the high-speed camera. Each specimen was x-rayed and autopsied after the test.

Test Results

The results of the sixteen impact tests are summarized in Table 2, where $Fimp$ is the impactor force, $Ftib$ is the tibial axial force when fracture occurred. Some dorsiflexion and a slight eversion were observed in every test. The dorsiflexion angle of the foot at failure is denoted by θ. The first peak in the tibial force was regarded as the failure load, as shown in the Figure 15.

Five tibial pylon fractures and ten calcaneal fractures were found while Cadaver #271L sustained no injury. The average values of the impactor force and the tibial axial force with fracture were 5132 N and 7645 N respectively. Figure 15 through 17 show the time histories of force and moment obtained in the case of Cadaver #28483L, showing a typical result in this series of tests. The impactor force and the tibial axial force, shown in Figure 15, were similar to each other except for an almost constant difference between them. The tibial axial force was higher than the impactor force because of the muscular preloading. The maximum tibial axial force appeared about 5 ms after the contact. The tensile force in the Achilles tendon, shown in Figure 16, was almost constant during the test. Figure 17 shows the tibial moment around X and Y axes, where a positive Mx implies lateral bending on the right leg and a positive My indicates plantarflexion. My ranged from 70 to 130 Nm in dorsiflexion whereas Mx was always acting in a single lateral direction. Mx was around 150 Nm in most of the tests.

One of the specimens with pylon fracture also had a lateral malleolar fracture and two of the ten calcaneal fractures were accompanied by a small crack in the talus. The lateral malleolar fracture suggests that the distal tibia was not necessarily compressed axially because of the slight eversion. Figure 18 shows an X-ray and an autopsy picture of Cadaver #715R which sustained a tibial pylon fracture. The calcaneus bones were uninjured in all of the five cases
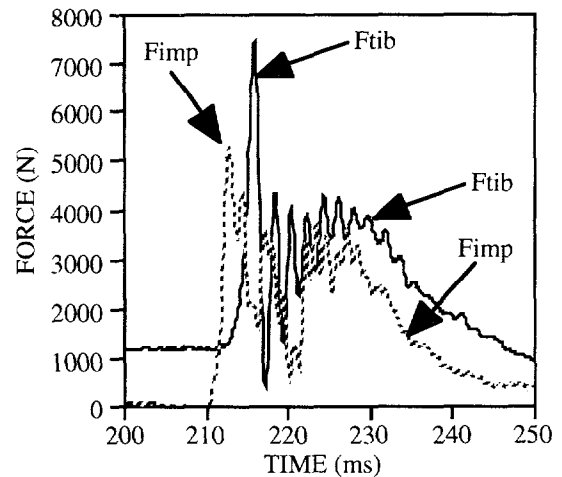
Figure 15. Impactor and Tibial Forces.
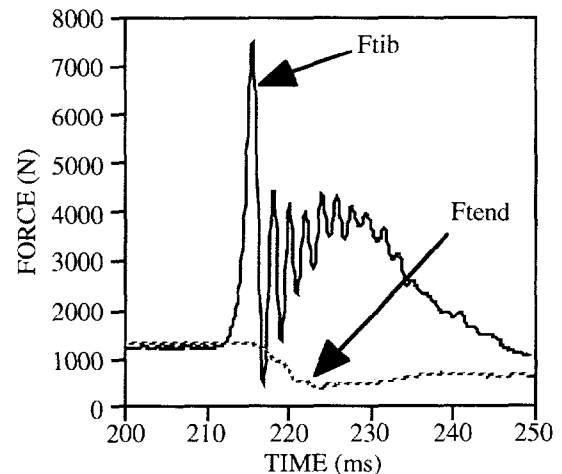
Figure 16. Tibial and Tendon Forces.
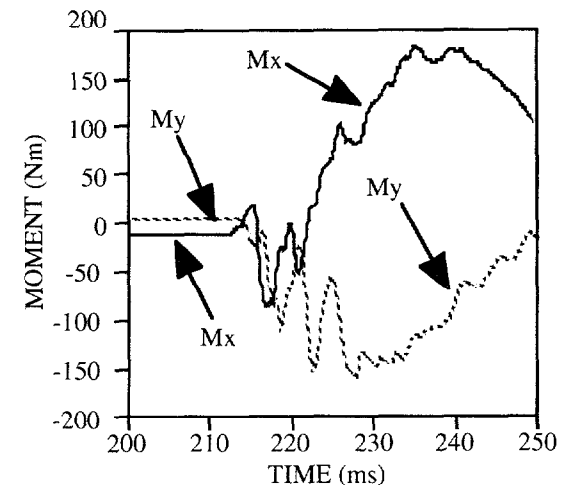
Figure 17. Tibial Moments.
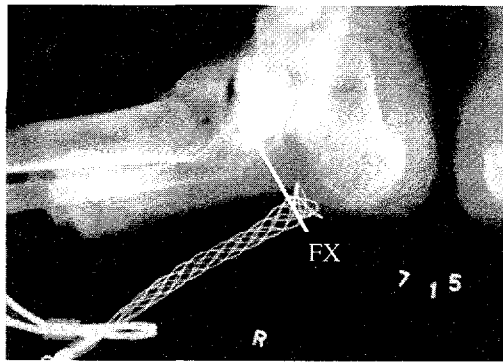
(a) X-ray Photograph
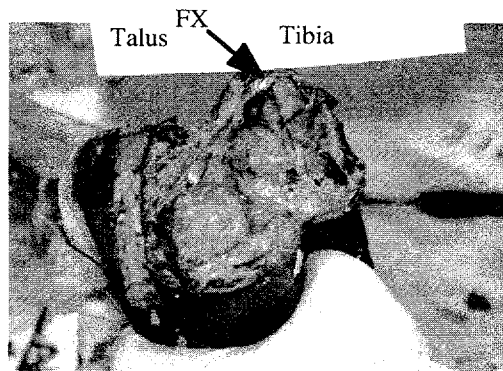
(b) Autopsy Photograph

Figure 18. CAD#715R (Pylon Fracture).

Right   Left
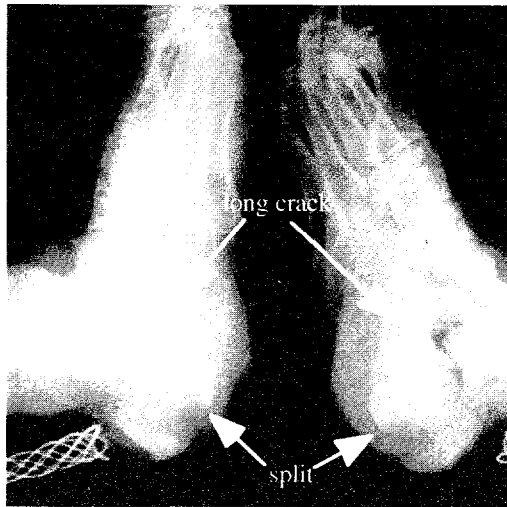
Figure 19. CAD#28443 (Calcaneal FX).

with pylon fractures. The small values of θ for ankle dorsiflexion means that the distal tibia was compressed very hard by the talus without causing a large dorsiflexion. The consequence is either a tibial pylon fracture or a calcaneal
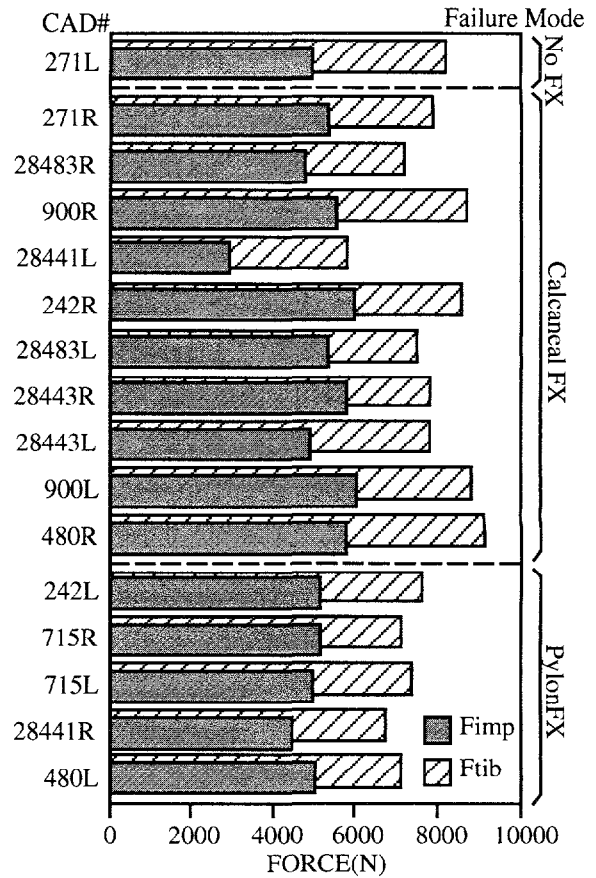
Figure 20. Failure Loads at Impactor and Tibia.

fracture. An X-ray of a typical calcaneal fracture is shown in Figure 19.

The common failure pattern in the calcaneus was a long crack from the bottom through the sinus tarsi (subtalar tunnel). There was another split-type fracture in the posterior side just under the tendon attachment point, which was found in some cases simultaneously with the first pattern. Both of them are primarily tension-type injuries. Failure forces are plotted in Figure 20 for the two types of fractures observed in this study. Cadaver #28441 was found to have advanced cervical carcinoma, which might be why its failure loads were lower than those of the other specimens despite the fact there was no indication of osteoporosis. The average impactor and tibial loads, excluding Cadaver #28441, for calcaneal fracture were 5483 N and 8115 N respectively while they were 5066 N and 7293 N respectively for pylon fracture. It is an unexpected result in that the failure load causing pylon fracture was lower than that of calcaneal fracture, as pylon fracture was supposed to occur at higher load, and bones are generally weaker under tensile loading. One reason is that the strength of bones is different between individuals. If the strength of these bones are close, two different fracture modes can occur under the same loading

1605

condition. Another possible explanation for occurrence of calcaneal fracture is that the tendon force was raised due to some reason such as the strain rate dependency of the material or the friction on the wire. The difference between the maximum impactor force and the maximum tibial axial force was approximately 2.6 kN in calcaneal fracture cases whereas it was about 2.2 kN in pylon fracture cases.

Looking back at previous work, an average tibial fracture load of 7830 N was proposed by Yoganandan (1996) and 7848 N by Begeman (1997). The impact velocity causing these fractures ranged from 4 to 6 m/s. Although the tibial fracture load in this study was almost the same as that reported previously, it was discovered that less impact force or lower impact velocity can cause tibial pylon fracture when muscular force is acting. Although muscular force is not always necessary to cause pylon fracture, it increases the injury risk compared to the relaxed case. The result is not inconsistent with the fact that there are cases where the driver's left leg or the passenger's legs sustained pylon fractures.

Future studies will focus on the threshold of tibial pylon fracture. It was not determined exactly because of the small number of specimens used and the majority of the specimens were female. The failure load is presently estimated at around 7 kN according to these test results. The impact point on the forefoot can be another dominant factor determining the fracture mode. Various impact conditions should be taken into account for a better understanding of the mechanism. In terms of methodology, numerical simulation using finite element models will be able to explain the mechanism of pylon fracture. Deformable elements are required to calculate stress and strain distribution in the bones of the foot. This will be the next effort in this research study.

CONCLUSION

1. Both muscular tension and external force due to intrusion can increase the axial force on the right tibia whereas the external force also determines the impact severity to the foot. The right tibia is subjected to preloading when the muscular force acts during braking.
2. Since the peaks in these forces appear at around 60 ms, the final extent of intrusion does not seem to be a major factor causing ankle/foot injuries.
3. The severity of external forces may be also affected by intrusion speed.
4. The calcaneus was the first contact area in the

Table 2. Test Results and Autopsy Report of Specimens

No.	CAD#	V(m/s)	Fimp(N)	Ftib(N)	θ (deg)	Autopsy
1	271R	3.62	5344	7801	2.8	Calcaneal FX(crack*)
2	271L	3.17	4932	8152	3.5	No Fracture
3	242R	3.99	5969	8549	1.8	Calcaneal FX(crack&split**)
4	242L	3.74	5179	7620	0.0	Pylon FX
5	715R	3.73	5116	7110	3.0	Pylon & Med. Malleolar FX
6	715L	3.31	4971	7349	1.5	Pylon FX
7	28483R	3.31	4791	7145	0.0	Calcaneal FX(crack)
8	28483L	3.59	5306	7437	0.0	Calcaneal FX(crack&split)
9	28443R	3.54	5786	7779	1.5	Calcaneal FX(crack&split)
10	28443L	3.17	4890	7759	3.0	Calcaneal(crack&split) & Talus FX
11	28441R	2.91	4462	6738	0.0	Pylon FX
12	28441L	2.37	2917	5737	0.0	Calcaneal(crack) & Talus FX
13	900R	3.60	5483	8654	0.0	Calcaneal FX(crack)
14	900L	3.73	6012	8803	2.0	Calcaneal FX(crack&split)
15	480R	3.76	5765	9108	0.0	Calcaneal FX(crack&split)
16	480L	3.68	4996	7091	0.0	Pylon FX

* a long crack from the bottom of the calcaneus through the sinus tarsi.
** split-type fracture in posterior side of the calcaneus just under the tendon attachment point.

MADYMNO simulation. It could be the reason why calcaneal fracture is frequently seen in real crashes.

5. The tibial axial force was always higher than the impactor force in this study because of the muscular preloading by the Achilles tendon.

6. Five tibial pylon fractures and ten calcaneal fractures were found out of sixteen specimens tested.

7. The calcaneus was intact in the five cases in which pylon fractures occurred.

8. A long crack from the bottom of the calcaneus through the sinus tarsi and a split in the posterior side were observed in calcaneal fractures.

9. The average failure loads measured at the tibial end were 8115 N for calcaneal fractures and 7293 N for pylon fractures (excluding Cadaver# 28441).

10. A high impact force or high impact velocity is not necessary to cause tibial pylon fracture when a muscular force is active.

ACKNOWLEDGMENT

REFERENCES

Morgan, R., Eppinger, R. (1991); Ankle Joint Injury Mechanism for Adults in Frontal Automotive Impact, 35th Stapp Car Crash Conference, SAE912902.

Crandall, J., Klisch, S., Klopp, G., Sieveka, E., Pilkey, W., Martin, P. (1994); Research Program to Investigate Lower Extremity Injuries, SAE Paper 940711.

Otte, D., Rheinbaben, H., Zwipp. H. (1992); Biomechanics of Injuries ot the Foot and Ankle Joint of Car Drivers and Improvements for an Optimal Car Floor Development, 36th Stapp Car Crash Conference, SAE 922514.

Thomas, P., Charles, J., Fay, P. (1995); Lower Limb Injuries - The Effect of Intrusion, Crash Severity and the Pedals on Injury Risk and Injury Type in Frontal Collisions, Proc. 39th Stapp Car Crash Conference, SAE 952728.

Begeman, P., Prasad, P. (1990); Human Ankle Impact Response in Dorsiflexion, Proc. 34th Stapp Car Crash Conference, SAE 902308.

Begeman, P., Balakrishnan, P., Levine, R., King, A. (1993); Dynamic Human Ankle Response to Inversion and Eversion, Proc. 37th Stapp Car Crash Conference, SAE 933115.

Yoganandan, N., Pintar, F., Boynton, M., Begeman, P., Prasad, P., Kuppa, S., Morgan, R. and Eppinger, R. (1996); Dynamic Axial Tolerance of the Human Foot-Ankle Complex, Proc. 40th Stapp Car Crash Conference, SAE 962426.

Klopp, G., Crandall, J., Hall, G., Pilkey,W., Hurwitz, S., Kuppa, S. (1997); Mechanisms of Injury and Injury Criteria for the Human Foot and Ankle in Dynamic Axial Impacts to the Foot, Proc. IRCOBI Conference, 73-86.

Levine, Robert S. (1986); A Review of the Long-Term Effects of Selected Lower Lim Injuries, SAE Paper 860501.

Begeman, P. and Paravasthu N. (1997); Static and Dynamic Compression Loading of the Lower Leg, Proc. 7th Injury Prevention Through Biomechanics Symposium, 103.

Roberts, David P. (1987); Injury Mechanism of Axial Load to Leg, 15th International Workshop on Human Subjects for Biomechanical Research, 45-61.

Lestina, C., Kuhlman, T., Keats, T., Alley, R. (1992); Mechanisms of Fracture in Ankle and Foot Injuries to Drivers in Motor Vehicle Crashes, Proc. 36th Stapp Car Crash Conference, SAE 922515.

Armstrong, R., Waters, H., Stapp, J. (1968); Human Muscular Restraint During Sled Deceleration, Proc. 12th Stapp Car Crash Conference, SAE 680793.

Frampton, R., Hill, J., Mackay, G. (1995); Leg Injury Risk in Frontal Collisions, SAE Paper 950499.

Sakurai, M. (1996); An Analysis of Injury Mechanisms for Ankle/Foot Region in Frontal Offset Collisions, Proc. 40th Stapp Car Crash Conference, SAE 962429.

Pattimore, D., Ward, E., Thomas, P., Bradford, M. (1991); The Nature and Cause of Lower Limb Injuries in Car Crashes, 35th Stapp Car Crash Conference, SAE 912901.

Portier, L., Petit, P., Trosseille, X., Tarriere, C., Lavaste, F. (1995); Experimental Research Program on Lower Leg Injuries in Frontal Car Crashes, Proc. International Conference on Pelvic and Lower Extremity Injuries (PLEI).

Klopp, G., Crandall, J., Sieveka, E., Pilkey, W. (1995); Simulation of Muscle Tensing in Pre-Impact Bracing, Proc. IRCOBI Conference, 171-182.